Calibrating the Galactic Cepheid Period–Luminosity Relation from the Maximum-likelihood Technique

Yaroslav A. Lazovik[1,2] and Alexey S. Rastorguev[1,2]
[1] Lomonosov Moscow State University, Faculty of Physics, 1 Leninskie Gory, bldg.2, Moscow, 119991, Russia; yaroslav.lazovik@gmail.com
[2] Lomonosov Moscow State University, Sternberg Astronomical Institute, 13 Universitetskiy prospect, Moscow, 119234, Russia

Abstract

We present a realization of the maximum-likelihood technique, which is one of the latest modifications of the Baade–Becker–Wesselink method. Our approach is based on nonlinear calibrations of the effective temperature and bolometric correction, which take into account metallicity and surface gravity. It allows one to estimate the key Cepheid parameters, the distance modulus, and the interstellar reddening, combining photometric and spectroscopic data (including the effective temperature data). This method is applied to a sample of 44 Galactic Cepheids for which multiphase temperature measurements are available. The additional data correction is performed to subtract the impact of the component in binary/multiple systems. We also study the effect of shock waves, whose presence in the stellar atmosphere distorts the observational data and leads to systematic errors in the obtained parameters. We determine the optimal restriction on the input data to eliminate this effect. This restriction provides accurate period–radius and period–luminosity relations that are consistent with the results in previous studies. We found the following relations: $\log R = (0.68 \pm 0.03) \cdot \log P + (1.14 \pm 0.03)$, $M_v = -(2.67 \pm 0.16) \cdot (\log P - 1) - (4.14 \pm 0.05)$.

Unified Astronomy Thesaurus concepts: Cepheid variable stars (218); Cepheid distance (217)

1. Introduction

In modern astronomy Cepheid variables play a particularly important role. Since the discovery of the period–luminosity relation (PL, or also Leavitt law, Leavitt 1908; Leavitt & Pickering 1912) in 1912, these stars have become the key objects in the context of extragalactic distance-scale calibration and Hubble constant estimation (Riess et al. 2011, 2018, 2019). Decades of work led to great progress in this field of research owing to both theory and observations. Technology development provided more accurate observational data while fundamental research in astrophysics prepared a comprehensive theoretical background. However, calibrating the precise PL relation still remains a priority in astronomy.

Nowadays there are several methods used to solve this task and each of them has its own features and limitations. One of the most commonly used methods is trigonometric parallax, which is inextricably linked to the Gaia mission (Gaia Collaboration et al. 2018). However, the derived PL relation strongly depends on the parallax zero-point offset (Groenewegen 2018). Additionally, in the case of Gaia DR2 data, the astrometric precision achieved for close systems is low because such systems are not resolved, regardless of secondary brightness (Ziegler et al. 2018). The capabilities of trigonometric parallax are very sensitive to the characteristic distance values, as the astrometric precision delivered for far located stars is much lower. The distances obtained for Cepheids in open clusters are more reliable, but sometimes it is not straightforward to confirm cluster membership. Eventually, the limited number of such objects prevents calibrating a precise PL relation based on cluster Cepheids only.

In light of the above, the Baade–Becker–Wesselink (BBW; Baade 1926; Becker 1940; Wesselink 1946) method stands out because it is devoid of the abovementioned flaws. The universality of this method makes it the only reasonable way to establish an extragalactic distance scale with Cepheid variables. Nowadays the BBW method is more complicated than it was in the original works, and many different modifications have been proposed, among which the infrared surface-brightness (IRSB; Barnes & Evans 1976) technique deserves special attention as the most frequently used implementation. Nevertheless, it is not the only approach. In this study we present another modification of the BBW method, namely the maximum-likelihood (ML) technique, whose basics were first described by Balona (1977), which is why we also call it the Baade–Becker–Wesselink–Balona method. The generalization of this method has been developed by Rastorguev and Dambis (RD version; Rastorguev & Dambis 2011). The key feature of our approach is using the multiphase effective temperature data to independently determine the stellar distance and the main physical parameters, such as radius and luminosity, as well as the amount of interstellar reddening. IRSB and ML techniques have many common features since they both rely on an identical theoretical framework, but consider the same task from different angles. It will be demonstrated that the ML technique has advantages over the IRSB method. Today the capabilities of our approach are limited by the amount of observational material. Here we work with a relatively small sample consisting of 44 Galactic Cepheids for which multiphase effective temperature variations are available. However, it will be shown that the ML technique has the potential to become a useful tool in the context of distance-scale calibration, as it is physically based and independent of other geometric techniques used to investigate the intrinsic properties of Cepheids. By comparing these results we are certain to learn more about Cepheids as physical systems locally and learn more about the physical expansion of the universe by the application of Cepheids (and their PL relation) to the more distant universe.

This paper is structured as follows. In the next section we emphasize the theoretical basis of the ML method. In Section 3 we dwell on the observational data and data reduction. The
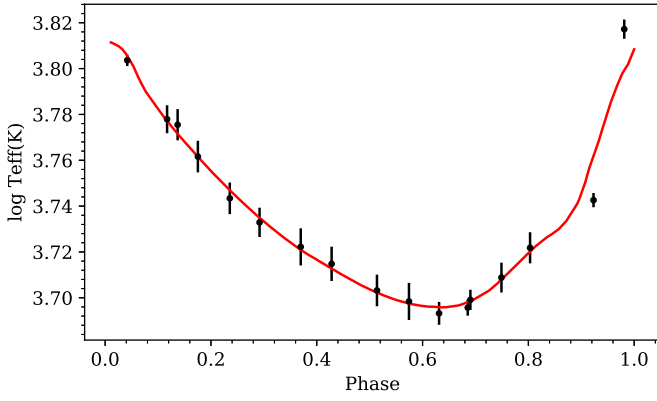
Figure 1. Effective temperature curve for CD Cyg. Dots with error bars: effective temperatures from Luck (2018). Red solid line: the model curve calculated using the relation from the present work (see Rastorguev et al. 2019).

results are presented in Section 4, and the discussion is presented in Section 5. Finally, we summarize our work in Section 6.

2. Method

We now briefly outline the RD version of the ML technique (see Rastorguev & Dambis 2011; Rastorguev et al. 2013 and Rastorguev et al. 2019 for details). The central equation of this method is the relation for the model light curve, which can be derived from the Stefan–Boltzmann law and the relation between absolute magnitude and apparent magnitude:

$$m = Y - 5 \cdot \log \frac{R}{R_\odot} + \Psi, \tag{1}$$

where Y is a constant depending on stellar apparent distance:

$$Y = (m - M)_{\text{app}} + M_{\text{bol}\odot} + 10 \cdot \log T_{\text{eff}\odot}, \tag{2}$$

and Ψ is a function of normal color index $\text{CI}_0 = \text{CI} - \text{CE}$ (CE is the color excess):

$$\Psi(\text{CI}_0) = \text{BC} + 10 \cdot \log T_{\text{eff}}, \tag{3}$$

where BC is the bolometric correction. The value of Ψ can be expressed from nonlinear calibrations $\text{BC}(\text{CI}_0)$ and $\log T_{\text{eff}}(\text{CI}_0)$:

$$\text{BC} = a_0 + \sum_{k=1}^{N_1} a_k \text{CI}_0^k, \tag{4}$$

$$\log T_{\text{eff}} = b_0 + \sum_{k=1}^{N_2} b_k \text{CI}_0^k. \tag{5}$$

Note that we also take into account the impact of surface gravity and metallicity, as the coefficients b_k in Equation (5) depend on $\log g$ and [Fe/H]. Both $\log g$ and [Fe/H] are assumed as constant parameters.

Requiring the best agreement between the observed values of the effective temperature and the model values computed from Equation (5), we estimate the color excess ($E(B - V)$), which is then used to derive Ψ. We initially employed the $\text{BC}((B - V)_0)$ relation from Flower (1996) and the $\log T_{\text{eff}}((B - V)_0)$ relation from Bessell et al. (1998). After estimating $E(B - V)$ values for 33 Cepheids we recalibrated $\log T_{\text{eff}}((B - V)_0)$ relation, treating Bessell's coefficients as the first approximation. The final $\log T_{\text{eff}}((B - V)_0)$ expression is

given by Rastorguev et al. (2019). An example of the effective temperature model curve for CD Cyg is presented in Figure 1.

We obtained the radius variation $\Delta R(\varphi)$, integrating radial-velocity curve over time:

$$\Delta R(\varphi) = -p \cdot \int_{\varphi_0}^{\varphi} (V_r(\varphi) - V_\gamma) \frac{P}{2\pi} d\varphi, \tag{6}$$

where p is the projection factor; $V_r(\varphi)$ is the radial velocity; V_γ is the systematic radial velocity; R_0 is the average radius value; P is the pulsation period; and φ is the current phase of the radial velocity curve. The main uncertainty of our method arises from the projection factor (p-factor) estimation. P-factor provides a conversion from radial to pulsation velocity. Nardetto et al. (2017) decomposes p-factor into three components: geometric projection factor (p_0), the atmospheric velocity gradient (f_{grad}), and the relative motion of the optical pulsating photosphere with respect to the corresponding mass elements (f_{o-g}). The authors propose different values of p-factor, and there is still no consensus concerning its correlation with the pulsation period (Nardetto et al. 2004, 2007, 2009; Groenewegen 2007). Moreover, for a given Cepheid, the projection factor may change during the pulsation cycle (Hindsley & Bell 1986; Gautschy 1987; Butler 1993; Sasselov & Karovska 1994; Sabbey et al. 1995). Today we lack quantitative theoretical estimates for such variations, which is why we neglect them. In the present work we adopt the relation from Nardetto et al. (2007):

$$p = 1.376 - 0.064 \cdot \log P. \tag{7}$$

The mean radius value is derived from the main Balona equation:

$$m = c_0 + \sum_{k=1}^{N_3} c_k \text{CI}^k - 5 \cdot \log(R_0 + \Delta R(\varphi)), \tag{8}$$

where c_k and R_0 are the unknown parameters.

Once we obtain the stellar color excess and radius, the apparent distance remains the only unknown parameter in the light curve equation (Equation (1)), which can be easily found using the least-squares method. The last step of our algorithm is calculating the absolute distance modulus:

$$(m - M)_0 = (m - M)_{\text{app}} - A, \tag{9}$$

where interstellar extinction A can be determined as $A_\lambda = R_\lambda \cdot E(B - V)$, where R_λ is the total-to-selective extinction ratio for the passband color pair considered ($R_v = 3.3$; Storm et al. 2004). Figure 2 shows the observed and model V-band light curves for CD Cyg.

As noted by Rastorguev et al. (2019), the outlined method and IRSB technique are based on the same theoretical material. However, if the IRSB technique can be considered as the simulation of radius changes, the ML technique simulates the light curve.

Contrary to IRSB technique, our method does not require preliminary color excess estimations. As explained by Madore et al. (2017), the errors in the reddening determinations are the factor that increases the dispersion of the existing PL relations. Moreover, we found that the effective temperature calibrations are very sensitive to the color excess variations, which is why it is important to be able to directly estimate the reddenings for individual objects to achieve high precision of the distance
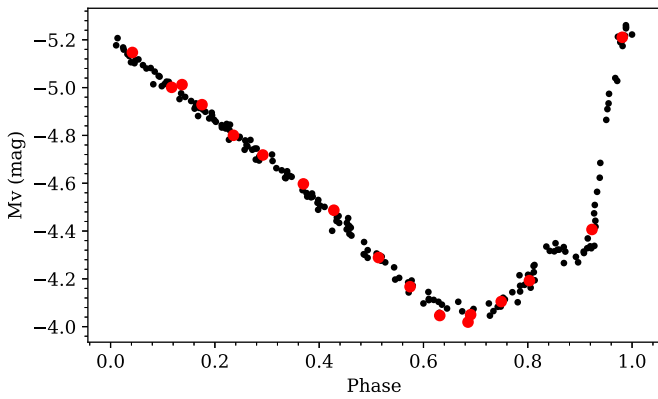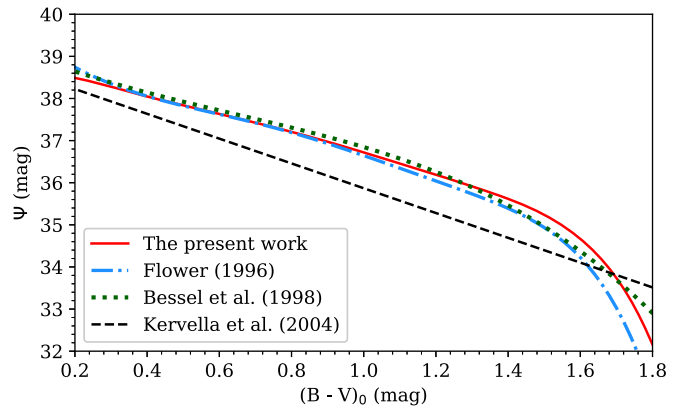
Figure 2. Light curves for CD Cyg. Black dots: the observed light curve shifted by the value of the apparent distance modulus. Red circles: values calculated from Equation (1).

Figure 3. IRSB and ML $\Psi(CI_0)$ calibrations for CD Cyg ($\log g = 1.30$; [Fe/H] = 0.15). Red solid line: relation used in the present work. Dashed–dotted blue line: relation from Flower (1996). Dotted green line: relation from Bessell et al. (1998). Dashed black line: relation from Kervella et al. (2004b).

Figure 4. Effective temperature curve for the binary Cepheid AW Per. Dots: effective temperatures from Luck (2018). Blue dashed line: the model curve corresponding to the uncorrected photometric data. Red solid line: the model curve corresponding to the corrected photometric data.

scale. Adopting gravity- and metallicity-dependent nonlinear calibrations leads to significantly different results with respect to the linear calibrations of the IRSB method. A comparison of the ML (Flower 1996; Bessell et al. 1998; the present work) versions with the IRSB version (Kervella et al. 2004b) of $\Psi(CI_0)$ calibration in the case of CD Cyg is depicted in Figure 3.

In addition, the results obtained with the IRSB method differ from the results of the present research simply because of our choice in favor of *B*-band photometry over traditionally used infrared photometry. This choice is justified by the fact that stellar radius, pulsation velocity, limb-darkening law, and projection factor are all wavelength-dependent (Marengo et al. 2003; Nardetto et al. 2009; Howarth 2011; Neilson et al. 2017). Given that the radial velocity measurements are related to the optical spectrum, solving the Balona equation (Equation (8)) with infrared photometry (corresponding to the different radius value), affected by the radiation of circumstellar gas, without any transformations would introduce errors into the final solution. For this reason, in this study, we settle on using data that corresponds to the single part of the spectrum and thus to the single radius value.

3. The Data

In this study we use extensive multicolor photoelectric and CCD photometry in *B* and *V* bands from Berdnikov (2008). As for spectroscopic data, the radial velocity measurements come from Gorynya et al. (1992, 1996, 1998, 2002), and the effective temperature and metallicity measurements are from Luck (2018). The data are cleaned as we identify and remove the data sets with the highest dispersion relative to the phase curve. We also exclude the observations corresponding to the earliest epochs to ensure that the observational data are synchronous in time to prevent any systematic errors coming from evolutionary period changes resulting in phase shifts between light, color, and radial-velocity variations. The period has been subsequently recalculated with the remaining data. For data interpolation we apply locally-estimated scatterplot smoothing (loess). We found that the loess regression algorithm provides smoother fits than a Fourier series, although this difference does not affect the final period–radius (PR) and PL relations.
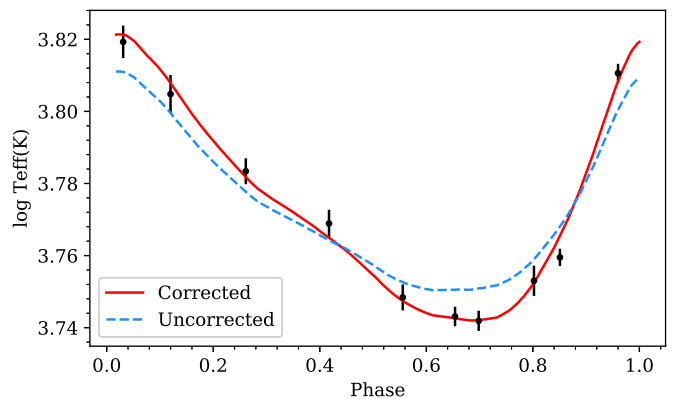
3.1. Cepheids in Binary and Multiple Systems

The full sample of stars considered in our research consists of 44 Galactic Cepheids, among which there are objects in binary and multiple systems. For these Cepheids an additional algorithm has been used to correct data from the impact of the component. First, we calculate the orbital parameters for the case of a binary system assuming minimal dispersion of residual velocities (corresponding to the pulsating motion) on the phase curve, after which we subtract orbital velocity from radial velocity data. Second, we subtract the impact of the brightest component from the photometric data. For this purpose, we take the spectral type of the component from Evans (1992, 1995), Evans et al. (2013), and Udalski & Evans (1993). With a given spectral type, using stellar parameters from Pecaut & Mamajek (2013) and the apparent distance modulus calculated with the initial (uncorrected) photometry, we compute *B* and *V* apparent magnitudes of the component, which allows us to correct the Cepheid light curves. Applying photometric correction does not lead to significant changes in the obtained stellar parameters for most of the Cepheids; however, there are several exceptions. The example of AW Per, shown in Figure 4, demonstrates that the effective temperatures calculated with a modified color index fit the observational data better. It is important to note that AW Per does not belong to

Table 1
Parameters of 44 Cepheid Variables Obtained with [0.00; 0.85] Phase Constraint

Cepheid	Sample	Binary	Fundamental Period (days)	$E(B-V)$ (mag)	$\langle R \rangle$ ($R_\odot$)	$\overline{M_v}$ (mag)	$(m-M)_0$ (mag)
AW Per	3	Yes	6.463	0.59 ± 0.01	39.2 ± 2.1	−3.34 ± 0.12	8.96 ± 0.17
BB Her	1	No	7.508	0.41 ± 0.02	56.2 ± 3.0	−3.85 ± 0.06	12.60 ± 0.06
BG Lac	2	No	5.332	0.29 ± 0.01	41.8 ± 2.1	−3.24 ± 0.07	11.18 ± 0.09
CD Cyg	1	No	17.074	0.59 ± 0.01	99.2 ± 2.0	−4.85 ± 0.04	11.87 ± 0.13
CF Cas	1	No	4.875	0.54 ± 0.02	44.3 ± 1.2	−3.34 ± 0.04	12.71 ± 0.12
CV Mon	3	No	5.379	0.69 ± 0.02	51.1 ± 2.7	−3.77 ± 0.12	11.79 ± 0.12
Delta Cep	1	Yes	5.366	0.09 ± 0.02	43.7 ± 2.3	−3.51 ± 0.06	7.17 ± 0.06
DL Cas	3	Yes	11.268	0.65 ± 0.02	87.0 ± 4.8	−4.82 ± 0.12	11.70 ± 0.18
DT Cyg	3	No	3.520	0.04 ± 0.01	42.3 ± 4.7	−3.63 ± 0.15	9.28 ± 0.15
Eta Aql	1	No	7.177	0.16 ± 0.01	56.3 ± 2.5	−3.92 ± 0.06	7.29 ± 0.07
FF Aql	3	Yes	6.297	0.27 ± 0.01	53.7 ± 7.6	−4.16 ± 0.18	8.64 ± 0.17
FM Aql	1	No	6.114	0.69 ± 0.02	52.2 ± 1.7	−3.79 ± 0.05	9.80 ± 0.15
FN Aql	1	No	9.482	0.48 ± 0.02	62.3 ± 1.4	−3.87 ± 0.04	10.67 ± 0.11
RS Ori	3	No	10.658	0.37 ± 0.01	72.7 ± 4.2	−4.60 ± 0.12	11.78 ± 0.14
RT Aur	1	No	3.728	0.06 ± 0.01	36.3 ± 1.6	−3.19 ± 0.06	8.44 ± 0.06
RX Aur	1	No	11.624	0.34 ± 0.01	72.5 ± 2.4	−4.50 ± 0.05	11.03 ± 0.09
RX Cam	2	Yes	7.912	0.55 ± 0.01	46.8 ± 2.7	−3.52 ± 0.08	9.39 ± 0.14
S Sge	1	Yes	8.382	0.17 ± 0.01	50.6 ± 1.2	−3.68 ± 0.04	8.74 ± 0.05
S Vul	1	No	68.438	1.15 ± 0.03	246.0 ± 8.1	−6.89 ± 0.08	12.06 ± 0.25
SS Sct	2	No	3.671	0.38 ± 0.03	36.3 ± 0.9	−3.13 ± 0.08	10.08 ± 0.11
SU Cyg	3	Yes	5.417	0.10 ± 0.02	49.8 ± 5.8	−3.98 ± 0.16	10.55 ± 0.16
SV Mon	1	No	15.235	0.29 ± 0.02	93.0 ± 1.7	−4.63 ± 0.06	11.93 ± 0.08
SV Vul	1	No	44.969	0.62 ± 0.03	192.0 ± 3.3	−6.08 ± 0.06	11.24 ± 0.14
T Mon	1	Yes	27.033	0.30 ± 0.05	119.7 ± 1.8	−4.95 ± 0.05	10.09 ± 0.08
T Vul	1	Yes	4.435	0.07 ± 0.02	39.8 ± 1.5	−3.33 ± 0.05	8.88 ± 0.05
TT Aql	1	No	13.755	0.59 ± 0.02	87.0 ± 1.9	−4.58 ± 0.06	9.77 ± 0.14
U Aql	3	Yes	7.024	0.44 ± 0.02	41.4 ± 1.7	−3.36 ± 0.14	8.33 ± 0.17
U Sgr	1	No	6.745	0.46 ± 0.01	48.9 ± 2.2	−3.62 ± 0.06	8.81 ± 0.11
U Vul	2	Yes	7.990	0.72 ± 0.02	40.9 ± 1.2	−3.35 ± 0.05	8.10 ± 0.15
V500 Sco	2	No	9.317	0.62 ± 0.03	62.1 ± 3.9	−4.05 ± 0.11	10.75 ± 0.17
VX Per	2	No	10.885	0.53 ± 0.02	79.7 ± 3.2	−4.60 ± 0.07	12.14 ± 0.13
W Gem	2	No	7.914	0.30 ± 0.03	47.1 ± 1.6	−3.60 ± 0.08	9.56 ± 0.10
W Sgr	1	Yes	7.595	0.13 ± 0.01	48.8 ± 1.5	−3.66 ± 0.06	7.92 ± 0.06
WZ Sgr	1	No	21.850	0.59 ± 0.03	120.2 ± 2.1	−5.03 ± 0.06	11.12 ± 0.14
X Cyg	1	No	16.386	0.35 ± 0.02	95.9 ± 2.5	−4.59 ± 0.07	9.84 ± 0.10
X Pup	3	No	25.965	0.53 ± 0.03	106.8 ± 2.8	−5.14 ± 0.12	11.93 ± 0.16
X Vul	1	No	6.320	0.85 ± 0.02	49.4 ± 2.0	−3.71 ± 0.05	9.73 ± 0.18
XX Sgr	2	No	6.424	0.58 ± 0.02	55.3 ± 2.7	−4.07 ± 0.07	11.02 ± 0.14
Y Lac	3	No	6.090	0.15 ± 0.02	48.7 ± 2.3	−3.77 ± 0.11	12.42 ± 0.12
Y Oph	2	No	17.128	0.78 ± 0.01	103.5 ± 3.0	−5.29 ± 0.06	8.87 ± 0.17
Y Sgr	2	No	5.773	0.23 ± 0.02	48.7 ± 1.1	−3.66 ± 0.04	8.62 ± 0.06
YZ Sgr	1	No	9.554	0.36 ± 0.01	55.7 ± 1.5	−3.81 ± 0.04	9.97 ± 0.08
Z Lac	1	Yes	10.886	0.49 ± 0.02	70.1 ± 1.1	−4.29 ± 0.06	11.10 ± 0.12
Zet Gem	3	No	10.150	0.07 ± 0.01	67.8 ± 3.3	−4.08 ± 0.12	7.71 ± 0.12

Note. The choice of [0.00; 0.85] phase restriction is explained in Section 4.2.

the list of 33 Cepheids that were used to refine $\log T_{\rm eff}((B-V)_0)$ calibration.

3.2. Samples

All Cepheids studied in this research are divided into three samples depending on the expected precision of the final parameters. Several factors have been taken into account, including the data quality and completeness, the presence of the component and its impact on the derived solution, and the pulsation type (overtone or fundamental). The first sample, corresponding to the Cepheids with the most reliable solutions, contains 23 objects, the second sample contains 10 objects, and the third sample contains 11 objects. The list of Cepheids,

sample membership, and the presence of a component are detailed in Table 1.

4. Results

4.1. Overtone Cepheids

Obtaining the PR relation allows one to identify overtone pulsators, which are shifted toward the lower period values relative to the linear fit. The fundamental period of these Cepheids can be calculated as a multiplication of the observed period and the constant coefficient (we assign it a value of 1.41). We suspect six objects to be the first overtone Cepheids, namely DL Cas, DT Cyg, FF Aql, RS Ori, SU Cyg, and Y Lac. Only two of them belong to the list of the first overtone pulsators in the General Catalogue of Variable Stars (Samus'

Table 2
Period–Radius Relations and Period–Luminosity Relations in the Form $\log(R) = a_r \cdot \log(P) + b_r$ and $M_v = a_v \cdot (\log(P) - 1) + b_v$, Respectively

Phase Restriction	Samples	a_r	b_r	SD_r	a_v	b_v	SD_v
No restriction [0.00; 1.00]	Sample 1	0.67 ± 0.03	1.15 ± 0.03	0.03	-2.51 ± 0.18	-4.19 ± 0.05	0.24
No restriction [0.00; 1.00]	Sample 1, 2	0.66 ± 0.03	1.17 ± 0.03	0.04	-2.50 ± 0.18	-4.22 ± 0.05	0.25
No restriction [0.00; 1.00]	Sample 1, 2, 3	0.65 ± 0.02	1.18 ± 0.03	0.04	-2.48 ± 0.16	-4.23 ± 0.04	0.27
Restriction [0.00; 0.85]	Sample 1	0.68 ± 0.03	1.14 ± 0.03	0.03	-2.65 ± 0.15	-4.13 ± 0.05	0.20
Restriction [0.00; 0.85]	Sample 1, 2	0.68 ± 0.03	1.14 ± 0.03	0.04	-2.67 ± 0.16	-4.14 ± 0.05	0.25
Restriction [0.00; 0.85]	Sample 1, 2, 3	0.68 ± 0.02	1.14 ± 0.03	0.05	-2.65 ± 0.15	-4.15 ± 0.04	0.30

Note. The coefficients are derived using the weighted least-squares method. SD_r refers to standard deviation of the period-radius relation, and SD_v refers to the standard deviation of the period–luminosity relation. We recommend relations computed for the combination of the first and the second samples.

et al. 2017), namely DT Cyg and FF Aql. The first overtone pulsation mode of DT Cyg is also suspected by Arellano Ferro (1984), while Udalski & Evans (1993) discuss the probability of FF Aql being an overtone pulsator. In addition to the above two stars, RS Ori is considered an overtone Cepheid in the Gaia DR2 catalog (Gaia Collaboration et al. 2018). Because we cannot clarify whether the shift in the PR diagram is caused by the different types of pulsation, by the uncertainties of the observational data, or by the possible evolutionary effects, these stars have been included in the third sample of objects. Moreover, the applicability of our calibrations to the overtone pulsators is questionable, which is why we suggest that the derived parameters of the stars listed above might contain additional errors.

Linear expressions of PR and PL relations are reported in Table 2.

4.2. Shock Waves

During the end of the pulsation cycle, which is related to the rebound around the minimum radius, shock waves arise in the atmosphere of Cepheids. Using high-resolution optical and infrared spectra and synthetic line profiles, Sabbey et al. (1995) has demonstrated that the presence of shock waves introduces asymmetries in the Cepheid line profiles. These asymmetries result in significant systematic errors in radial velocity and effective temperature measurements. Additionally, the calibrations adopted in this work might not be applicable to the phase region corresponding to the formation of shock waves. As a consequence, this phase region should be disregarded while calculating radius, color excess, and apparent distance modulus.

Figure 5 illustrates a mismatch between the pulsation curve obtained by a integrating radial velocity curve and radius estimations from the Balona equation (Equation (8)). The Balona equation, which is based on the $\log T_{\rm eff}\,(CI_0)$ relation, does not give satisfactory results during shock wave formation, indicating that this relation alone has its own application boundaries for Cepheid variables.

To obtain the application boundaries we consider the first sample of Cepheids and the upper limits in the range [0.80; 1.00] with a step of 0.01 to find out which constraint leads to the smallest scatter relative to the linear PL relation. Phase restrictions are applied to all Cepheids, despite the fact that some of them do not exhibit the presence of shock waves. Some authors (for example, Storm et al. 2011) disregard the [0.8, 1.0] phase interval to avoid using distorted data. However, we showed in Lazovik et al. (2019) that the phase constraint substantially affects the adopted PL relation, meaning that careful deduction of optimal restriction has to be provided. As
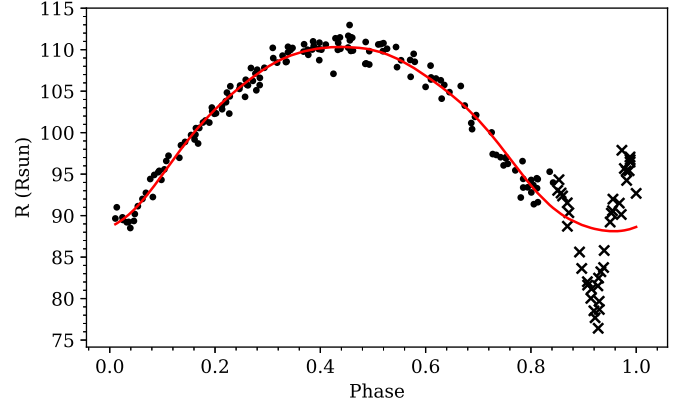
Figure 5. Pulsation curve for CD Cyg. Dots and crosses: radius estimations from Equation (8). Dots belong to the [0.00; 0.85] phase interval and crosses belong to the [0.85; 1.00] phase interval (disregarded region). Red solid line: integrated radial velocity curve.
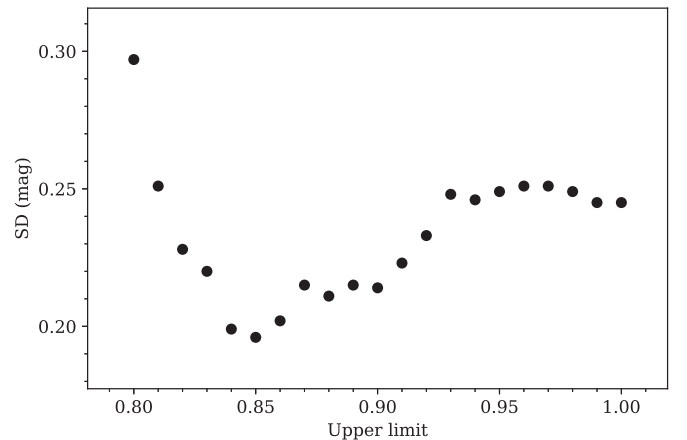

Figure 6. Standard deviation of the first sample of Cepheids in the PL diagram plotted against upper phase limit.

shown in Figure 6, excluding data inside [0.85; 1.00] minimizes spread in the PL diagram. Linear expressions of the PR and PL relations are given in Table 2, and PR and PL diagrams are plotted in Figure 7. We recall that the parameters calculated for Cepheids of the third sample are less reliable, therefore we recommend using relations derived from a combination of the first and the second samples.

4.3. Instability Strip

In the absence of observational and methodological uncertainties the scatter of the PL diagram represents the finite width of the instability strip in the color–magnitude diagram;
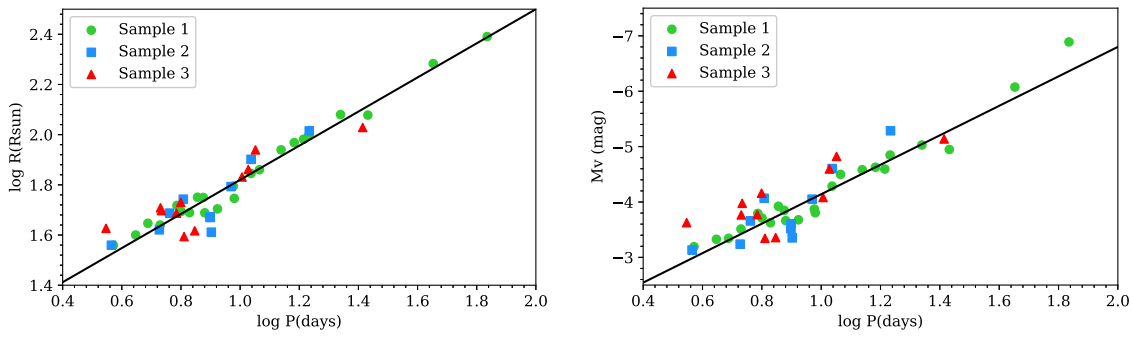
Figure 7. Left panel: period–radius diagram. Right panel: period–luminosity diagram in the *V* band. Green circles are the first sample of Cepheids, blue squares are the second sample, and red triangles are the third sample. The solid line is the linear fit.
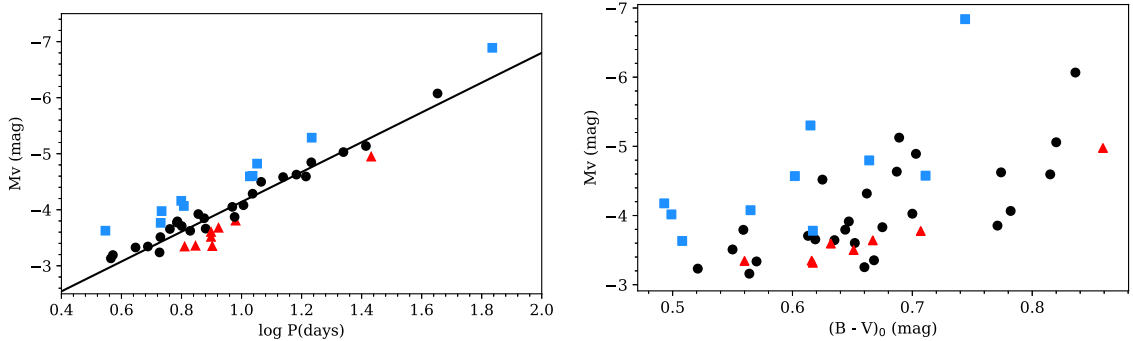
Figure 8. Left panel: period–luminosity diagram in the *V* band. Right panel: color–magnitude diagram. Blue squares and red triangles indicate Cepheids outside the 1σ limit in the PL diagram. Black circles indicate Cepheids inside the 1σ limit. $\sigma = 0.25$ mag.

the upper and lower envelope lines of the PL relation are traces of the blue and red boundaries of the instability region (Sandage 1958). The left panel of Figure 8 shows a period–luminosity diagram in which blue squares (red triangles) indicate relatively bright (faint) Cepheids. A color–magnitude diagram with the same objects and designations is depicted on the right. As expected, most of the bright Cepheids are on the blue edge. On the other hand, the Cepheids located lower the calculated PL relation do not represent the red edge. We do not yet have a clear explanation of this behavior, as it could be a result of some complicated evolutionary features as well as perturbations arising due to star–star interactions, since six out of eight faint Cepheids belong to binary/multiple systems.

5. Discussion

5.1. The Period–Radius Relation

Our PR relation is in good agreement with the results of previous studies (see Table 3). In particular, Gallenne et al. (2017) applied the SPIPS algorithm, which is an implementation of the BBW technique, to 29 LMC and 10 SMC Cepheids in order to derive all their main parameters and to calibrate the projection factor and the PR relation. The obtained coefficients are consistent with our estimations. Groenewegen (2007) derived a very similar PR relation after investigating five stars with known distances and measuring angular diameters as a function of the pulsation phase. In contrast, some studies (Turner & Burke 2002; Storm et al. 2004; Kervella et al. 2004a; Molinaro et al. 2011) propose a steeper PR relation. In our opinion, the difference is related to the impact of the projection factor. We note that the first two works are based on approaches that allow independent estimates of the *p*-factor, while in the latter four works the *p*-factor was adopted from

Table 3
Period–Radius Relations in the Form $\log(R) = a_r \cdot \log(P) + b_r$

References	a_r	b_r
Sachkov et al. (1998)	0.62 ± 0.03	1.23 ± 0.03
Bono et al. (1998)	0.655 ± 0.006	1.188 ± 0.008
The present work [0.00; 1.00]	0.66 ± 0.03	1.17 ± 0.03
Petroni et al. (2003)	0.676 ± 0.006	1.173 ± 0.008
The present work [0.00; 0.85]	0.68 ± 0.03	1.14 ± 0.03
Gallenne et al. (2017)	0.684 ± 0.007	1.135 ± 0.002
Groenewegen (2007)	0.686 ± 0.036	1.134 ± 0.034
Turner & Burke (2002)	0.747 ± 0.028	1.071 ± 0.025
Molinaro et al. (2011)	0.75 ± 0.03	1.10 ± 0.03
Kervella et al. (2004a)	0.767 ± 0.009	1.091 ± 0.011
Storm et al. (2004)	0.77 ± 0.02	1.05 ± 0.03

other studies. Theoretical studies (Bono et al. 1998; Petroni et al. 2003) also confirm our results. At the same time, Sachkov et al. (1998), applying Balona's method to the large sample of 62 Galactic Cepheids, computed a slightly shallower slope.

5.2. The Period–Luminosity Relation

Our results are compared with different studies in Table 4. Moreover, for better visualization we plotted our PL relation with the main relations from Table 4 in Figure 9. Each color represents the applied approach: black corresponds to trigonometric parallax, blue corresponds to the BBW method, and green corresponds to the expression based on Cepheids in open clusters. Our PL relation is highlighted in red. The results achieved using different methods and techniques are not self-consistent; there is considerable scatter in the PL diagram, with trigonometric relations being shallower than other relations. As we pointed out in Section 1, the precision of trigonometric

Table 4
Period–Luminosity Relations in the Form $M_v = a_v \cdot (\log(P) - 1) + b_v$

References	a_v	b_v	Method
Groenewegen (2018)	-2.243 ± 0.137	4.083 ± 0.118	Trigonometric parallax
Benedict et al. (2007)	-2.43 ± 0.12	-4.05 ± 0.02	Trigonometric parallax
The present work [0.00; 1.00]	-2.50 ± 0.18	-4.22 ± 0.05	ML
Gieren et al. (2018)	-2.690 ± 0.100	-3.981 ± 0.033	IRSB
The present work [0.00; 0.85]	-2.67 ± 0.16	-4.14 ± 0.05	ML
Storm et al. (2011)	-2.67 ± 0.10	-3.96 ± 0.03	IRSB
Fouqué et al. (2007)	-2.678 ± 0.076	-3.953 ± 0.023	IRSB
Kervella et al. (2004a)	-2.769 ± 0.073	-4.209 ± 0.075	IRSB
Molinaro et al. (2011)	-2.78 ± 0.11	-4.20 ± 0.11	CORS
Turner (2010)	-2.78 ± 0.12	-4.07 ± 0.10	Cepheids in clusters
Anderson et al. (2013)	-2.88 ± 0.18	-3.90 ± 0.16	Cepheids in clusters

parallax decreases rapidly with distance. Both the zero-point and the slope of the PL relations are correlated with the assumed parallax zero-point offset, whose influence does not allow improvement to the existing quality of distance-scale calibration (Groenewegen 2018). Nevertheless, in the range of small periods, which is related to predominantly close Cepheids with higher astrometric precision, our PL relation is in reasonable agreement with trigonometric parallaxes, especially with Hubble Space Telescope (HST) parallaxes (Benedict et al. 2007) Applying ML technique generally leads to brighter Cepheids and therefore to a longer distance scale, compared with the results provided by the IRSB method (Kervella et al. 2004a; Fouqué et al. 2007; Storm et al. 2011; Gieren et al. 2018) The latter is explained by the differences between the ML and IRSB techniques highlighted in Section 2. The best match is found between our relation and the relation from Molinaro et al. (2011).

The obtained results have global cosmological meaning, as the longer distance scale indicates the lower value of the Hubble constant, H_0. The current value of the Milky Way calibration used by Riess et al. (2019) relies on HST parallaxes (Benedict et al. 2007). The zero-point of the corresponding PL relation differs by 0.09 mag from the results presented in this study. Adopting such an offset in the Cepheid calibration would reduce the Hubble constant from $H_0 = 74$ km s^{-1} Mpc^{-1} to $H_0 = 71$ km s^{-1} Mpc^{-1}. However, we caution the reader against taking this estimate too seriously, as it is based on a simplifying assumption that all Cepheids are 0.09 mag brighter than was previously thought. Our main goal here is to demonstrate that there is evidence that supports the idea that the local value of the Hubble constant has to be lower. Future investigations are needed to support or disprove it.

5.3. The Distances

Our distance estimates are in excellent agreement with data from Mel'nik et al. (2015). Their procedure of calculating distances is based on the K-band period–luminosity relation from Berdnikov et al. (1996a) and an interstellar-extinction law derived by Berdnikov et al. (1996b). The distances from both studies, plotted against each other in Figure 10, are almost identical for the majority of Cepheids from the first two samples and even for several Cepheids from the third sample. Four suspected overtone Cepheids, namely Y Lac, DL Cas, RS Ori, and SU Cyg, have been disregarded in the linear regression because in Mel'nik et al. (2015) they are identified as the fundamental pulsators. The convergence is expressed by the following linear fit: $(m - M)_{\text{Berdnikov}} = (1.02 \pm 0.05) \cdot$

$(m - M)_{\text{Lazovik}} - (0.36 \pm 0.43)$, which is indistinguishable from the $y = x$ relation within the margin of error. The perfect match confirms the accuracy of our color excess evaluations. It is worth noting that the K-band extinction is negligible, while V-band extinction may be significant.

5.4. The Reddening System

As mentioned in Section 2, independent and direct reddening determinations for individual Cepheids are one of the main advantages of the ML technique over the other modifications of the BBW method. Nowadays the most conventional way to derive color excess implies observations of the early-type reference stars. These objects are plotted on the color–color diagram and compared with the relationships between spectral type and intrinsic color for standard (non-rotating, ZAMS) stars to obtain the color excess, which is subsequently transformed to fit the Cepheid spectral type.

The reddening system of Turner (2016) was established by the algorithm described above, using the Fernie (1963) transformation. A comparison of the reddenings derived in the present study with color excesses by Turner (2016) is depicted in Figure 11. There is moderate scatter as well as a reddening-dependent trend, which is indicated by the following regression fit: $(B - V)_{\text{Turner}} = (0.85 \pm 0.02) \cdot (B - V)_{\text{Lazovik}}$

$$+ (0.05 \pm 0.02).$$

We cannot be confident about where these discrepancies originate, but in our opinion the results of the ML technique are more reliable since our approach is more straightforward and based on the minimal amount of initial assumptions. This is not a critique of Turner (2016), however, we would like to point out the possible reasons for the inconsistencies in the color excess estimates.

First of all, we think that the Fernie (1963) reddening transformation should be updated. The calibration of a quantity that defines reddening of a late-type star relative to that of an early-type star is based on a scarce number of data points and does not take into account a possible dependence on metallicity. Second, the assumption that the reference stars can be approximated by zero-age zero-rotation main-sequence standard stars at solar metallicity is likely to be invalid in some cases. It is important to remember that B0-stars have relatively short main-sequence lifetimes, which is why a fraction of the reference stars may be evolved stars with different color–color relations. The effect of rotation is also significant, especially for intermediate- and high-mass stars, as it impacts the efficiency of transport and mixing of chemical elements, modifying the
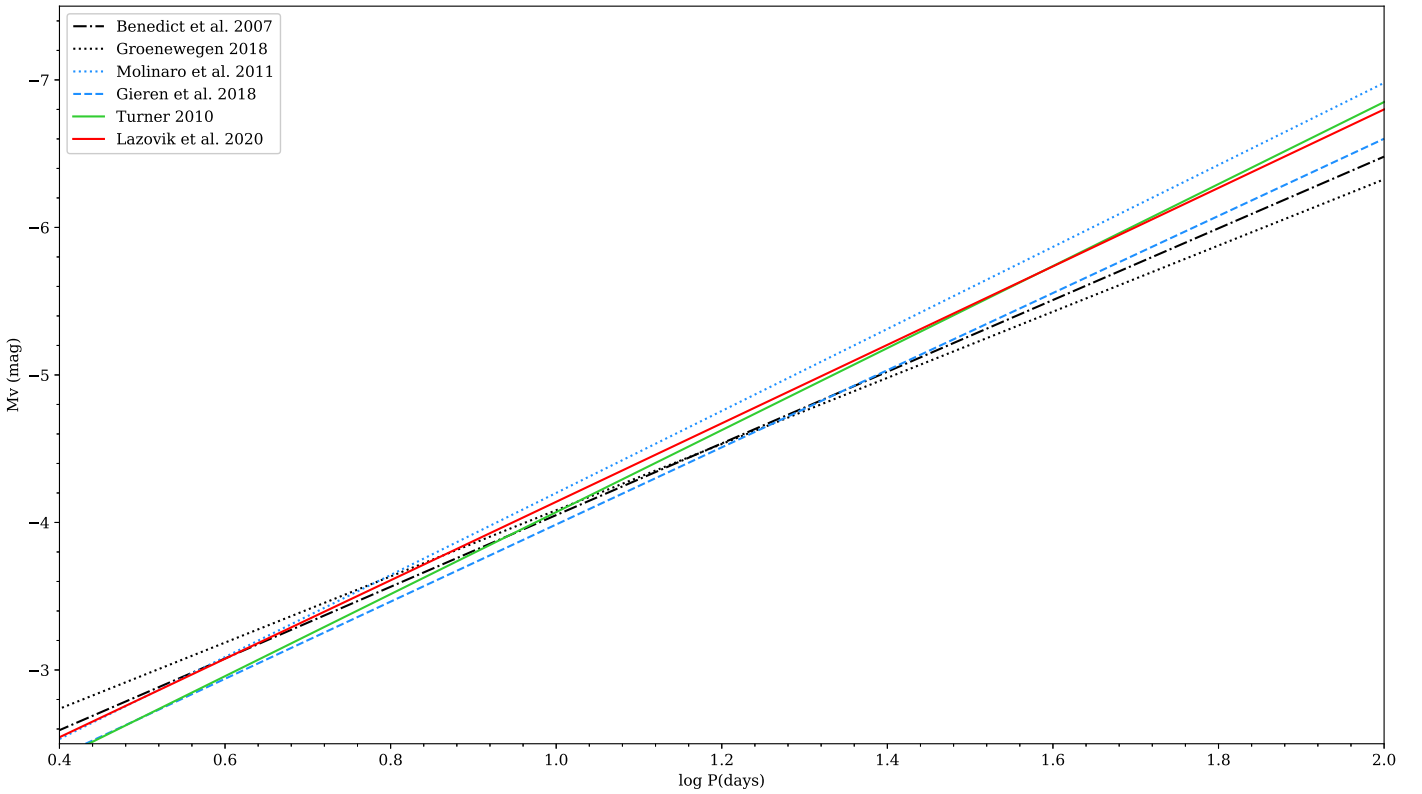
Figure 9. Period–luminosity relations obtained by different authors. Black lines show relations based on the trigonometric parallax method. Black dashed–dotted line: HST parallaxes (Benedict et al. 2007). Black dotted line: Gaia DR2 parallaxes (Groenewegen 2018). Blue lines show modifications of the Baade–Becker–Wesselink method. Blue dotted line: CORS method (Molinaro et al. 2011). Blue dashed line: IRSB method (Storm et al. 2011). Green solid line: PL relation obtained using Galactic Cepheids in open clusters and groups by Turner (2010). Red solid line: PL relation from the present work (obtained with phase limitation).
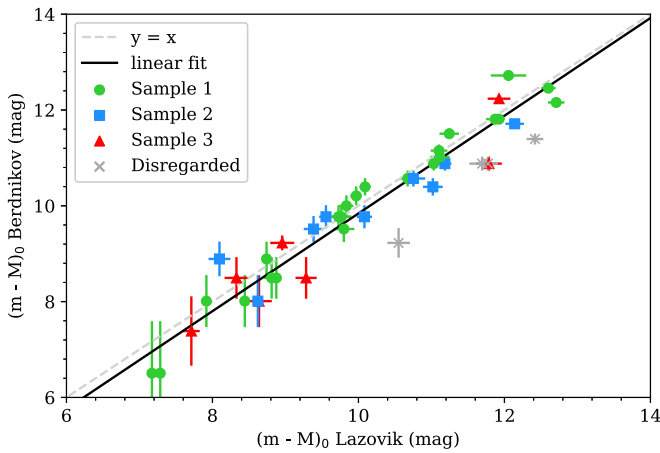
Figure 10. A comparison of the obtained distances and the distances from Mel'nik et al. (2015). Marker designations are the same as those in Figure 7, and gray crosses represent the overtone Cepheids that have been disregarded in the fit for reasons mentioned in the text. Gray dashed line: $y = x$. Black solid line: linear fit.
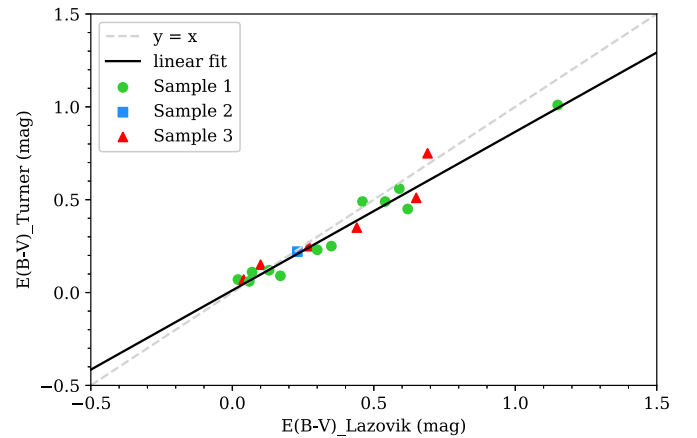

Figure 11. A comparison of the obtained color excesses with a reddening compilation from Turner (2016). Marker designations are the same as those in in Figure 7. Gray dashed line: $y = x$. Black solid line: linear fit.

internal stellar structure (Heger & Langer 2000; Heger et al. 2004; Mathis & Zahn 2004; Deal et al. 2020). Finally, the determination of the reddening law appears to be an essential and complicated task. Cardelli et al. (1989) finds large systematic differences in extinction for lines of sight with considerably different values of R_v, spanning from 2.60 to 5.60. The enormous range of properties exhibited by UV extinction in the Milky Way was also discussed by Fitzpatrick (1999) and Fitzpatrick & Massa (2007). It has been found that the properties of Milky Way extinction are not well determined

(Fitzpatrick 1999) and infrared through ultraviolet Galactic extinction curves have scatter too large to be considered a simple one-parameter family (Fitzpatrick 2004). Moreover, even for a given cluster the range of R_v values can be broad.

It is useful to dwell on the two objects for which the biggest deviations in color excess are found, namely S Vul and SV Vul (the corresponding deviations are 0.14 and 0.17 mag, respectively). These objects are the long-period Cepheids that were previously thought to be located in two star-forming associations, namely Vul OB1 and Vul OB2. Such associations, as well as the embedded clusters and groups, are commonly characterized by a substantial differential extinction,
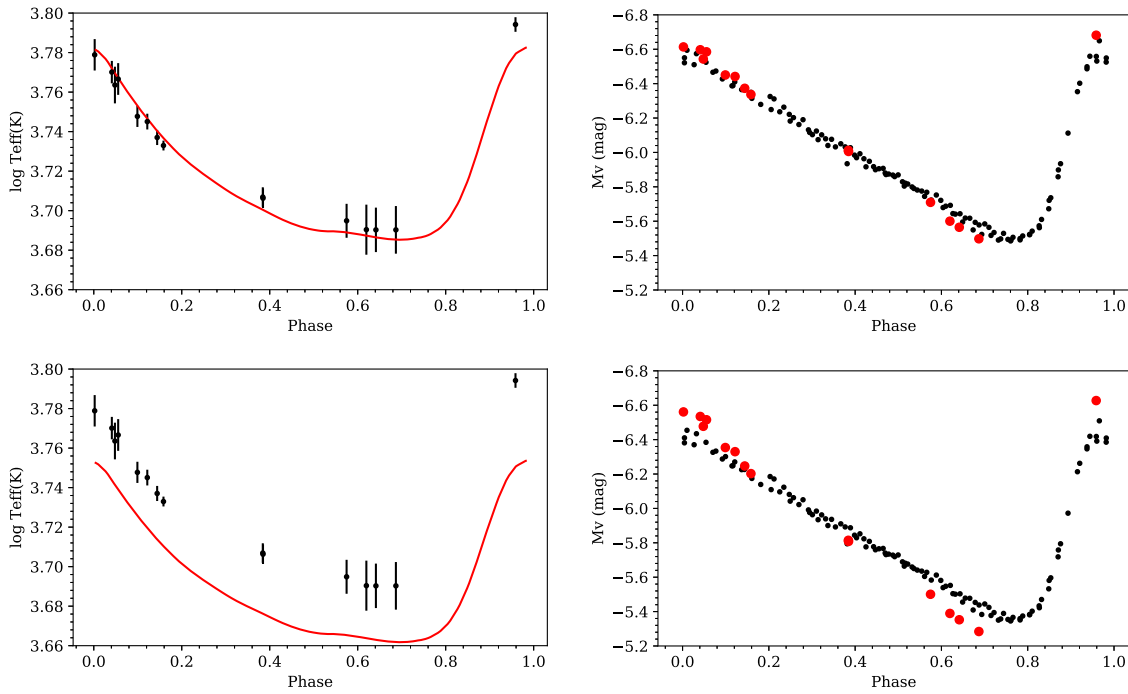
Figure 12. Left column: effective temperature curves for SV Vul. Marker designations are the same as those in Figure 1. Right column: light curves for SV Vul. Marker designations are the same as those in Figure 2. The top row corresponds to $E(B - V) = 0.62$ from the present study. The bottom row corresponds to $E(B - V) = 0.45$ from Turner (2016).

which might cause errors in the derived space reddenings. Recent studies (Negueruela et al. 2020) suggest that SV Vul is a member of another cluster, Alicante 13. Their results cast doubt on the classical view of two separate associations, Vul OB1 and Vul OB2, projected over the same region. Instead, supposed members of Vul OB1 and Vul OB2 may be distributed over a wide range of distances, making the classical approach of reddening estimation even more complicated.

The sensitivity of the effective temperature curve to the color excess variation in the case of SV Vul is illustrated on the left side of Figure 12. Adopting the reddening value from Turner (2016) leads to a discrepancy between the calibrated and observed values of the effective temperature, which is larger than the margin of errors. Moreover, the shape of the light curve calculated from Equation (1) with the color excess from Turner (2016) does not reproduce the shape of the observed light curve as well as the analogous curve calculated with the color excess from the present work (the right side of Figure 12). The choice of reddening does not affect radius estimation, since the Balona equation (Equation (8)) includes only observed values of color index. Adopting $E(B - V) = 0.45$ from Turner (2016) will slightly change the value of absolute magnitude from $\overline{M_v} = -6.08 \pm 0.05$ to $\overline{M_v} = -5.94 \pm 0.10$.

At the same time, S Vul and SV Vul, like the majority of long-period Cepheids, undergo fast period variations, which is why careful data reduction has to be provided to obtain smooth phase curves. Several data sets have been removed to make the remaining data converge with the single period value. For this reason, period variation arises as an extra source of errors in the ML determination of reddening, whose impact is difficult to assess.

6. Summary

In this study we have demonstrated the main features of the ML technique, which was originally developed by Balona (1977) and then modified by Rastorguev & Dambis (2011). The method combines effective temperature data with light, color, and radial velocity variations to determine the amount of interstellar reddening, to compute the key parameters of Cepheids, including radius and absolute magnitudes, and to estimate the absolute distance modulus. Applying this method to 44 Galactic Cepheids allows us to obtain the following period-radius and period–luminosity relations:
$\log R = (0.68 \pm 0.03) \cdot \log P + (1.14 \pm 0.03)$,
$M_v = -(2.67 \pm 0.16) \cdot (\log P - 1) - (4.14 \pm 0.05)$.

Our results are generally in good agreement with previous works. The period-radius relation is confirmed by theoretical studies (Petroni et al. 2003) and consistent with empirical works (Groenewegen 2007; Gallenne et al. 2017). The period–luminosity relation supports findings from Molinaro et al. (2011) and is compatible with HST parallaxes (Benedict et al. 2007), although it supports a slightly brighter Cepheid calibration and thus a larger distance scale than the IRSB technique and HST parallaxes.

The possibilities of the ML technique are far from being exhausted. Our next steps depend on future data. Currently, the biggest limitation arises from the number of Cepheids with multiphase effective temperature measurements; in the future, however, we will hone this list so that the obtained relations have higher precision. This is relevant to long-period variables because at the moment the group of Cepheids in our research contains only five objects with a fundamental period exceeding 20 days. The lack of such objects prevents us from reducing the uncertainty in the final PR and PL relations. We would like to apply our approach to SMC and LMC Cepheids to show that our method can reach extragalactic objects. Using multiband

photometry will provide new prospects for moving toward and improving the quality of distance-scale calibration.

ORCID iDs

Yaroslav A. Lazovik ⓘ https://orcid.org/0000-0001-6821-5006

References

Anderson, R. I., Eyer, L., & Mowlavi, N. 2013, MNRAS, 434, 2238
Arellano Ferro, A. 1984, MNRAS, 209, 481
Baade, W. 1926, AN, 228, 359
Balona, L. A. 1977, MNRAS, 178, 231
Barnes, T. G., & Evans, D. S. 1976, MNRAS, 174, 489
Becker, W. 1940, ZAp, 19, 289
Benedict, G. F., McArthur, B. E., Feast, M. W., et al. 2007, AJ, 133, 1810
Berdnikov, L. N., Vozyakova, O. V., & Dambis, A. K. 1996a, AstL, 22, 839
Berdnikov, L. N., Vozyakova, O. V., & Dambis, A. K. 1996b, AstL, 22, 334
Berdnikov, L. N. 2008, yCat, 285, 0
Bessell, M. S., Castelli, F., & Plez, B. 1998, A&A, 333, 231
Bono, G., Caputo, F., & Marconi, M. 1998, ApJL, 497, L43
Butler, R. P. 1993, ApJ, 415, 323
Cardelli, J. A., Clayton, G. C., & Mathis, J. S. 1989, ApJ, 345, 245
Deal, M., Goupil, M. J., Marques, J. P., Reese, D. R., & Lebreton, Y. 2020, A&A, 633, A23
Evans, N. E., Bond, H. E., Schaefer, G. H., et al. 2013, AJ, 146, 93
Evans, N. R. 1992, ApJ, 384, 220
Evans, N. R. 1995, ApJ, 445, 393
Fernie, J. D. 1963, AJ, 68, 780
Fitzpatrick, E. L. 1999, PASP, 111, 63
Fitzpatrick, E. L., & Massa, D. 2007, ApJ, 663, 320
Fitzpatrick, E. L. 2004, in ASP Conf. Ser. 309, Astrophysics of Dust, ed. A. N. Witt, G. C. Clayton, & B. T. Draine (San Francisco, CA: ASP), 33
Flower, P. J. 1996, ApJ, 469, 355
Fouqué, P., Arriagada, P., Storm, J., et al. 2007, A&A, 476, 73
Gaia Collaboration, Brown, A. G. A., Vallenari, A., et al. 2018, A&A, 616, A1
Gallenne, A., Kervella, P., Mérand, A., et al. 2017, A&A, 608, A18
Gautschy, A. 1987, VA, 30, 197
Gieren, W., Storm, J., Konorski, P., et al. 2018, A&A, 620, A99
Gorynya, N. A., Irsmambetova, T. R., Rastorgouev, A. S., & Samus, N. N. 1992, SvAL, 18, 316
Gorynya, N. A., Samus', N. N., Rastorguev, A. S., & Sachkov, M. E. 1996, AstL, 22, 175
Gorynya, N. A., Samus', N. N., Sachkov, M. E., et al. 1998, AstL, 24, 815
Gorynya, N. A., Samus, N. N., Sachkov, M. E., et al. 2002, yCat, 3229, 0
Groenewegen, M. A. T. 2007, A&A, 474, 975
Groenewegen, M. A. T. 2018, A&A, 619, A8

Heger, A., & Langer, N. 2000, ApJ, 544, 1016
Heger, A., Woosley, S. E., Langer, N., & Spruit, H. C. 2004, in IAU Symp. 215, Stellar Rotation, ed. A. Maeder & P. Eenens (San Francisco, CA: ASP), 591
Hindsley, R., & Bell, R. A. 1986, PASP, 98, 881
Howarth, I. D. 2011, MNRAS, 418, 1165
Kervella, P., Bersier, D., Mourard, D., et al. 2004b, A&A, 428, 587
Kervella, P., Bersier, D., Mourard, D., Nardetto, N., & Coudé du Foresto, V. 2004a, A&A, 423, 327
Lazovik, Y. A., Rastorguev, A. S., Zabolotskikh, M. V., & Gorynya, N. A. 2019, arXiv:1911.13102
Leavitt, H. S. 1908, AnHar, 60, 87
Leavitt, H. S., & Pickering, E. C. 1912, HarCi, 173, 1
Luck, R. E. 2018, AJ, 156, 171
Madore, B. F., Freedman, W. L., & Moak, S. 2017, ApJ, 842, 42
Marengo, M., Karovska, M., Sasselov, D. D., et al. 2003, ApJ, 589, 968
Mathis, S., & Zahn, J. P. 2004, A&A, 425, 229
Mel'nik, A. M., Rautiainen, P., Berdnikov, L. N., Dambis, A. K., & Rastorguev, A. S. 2015, AN, 336, 70
Molinaro, R., Ripepi, V., Marconi, M., et al. 2011, MNRAS, 413, 942
Nardetto, N., Fokin, A., Mourard, D., et al. 2004, A&A, 428, 131
Nardetto, N., Gieren, W., Kervella, P., et al. 2009, A&A, 502, 951
Nardetto, N., Mourard, D., Mathias, P., Fokin, A., & Gillet, D. 2007, A&A, 471, 661
Nardetto, N., Poretti, E., Rainer, M., et al. 2017, A&A, 597, A73
Negueruela, I., Dorda, R., & Marco, A. 2020, MNRAS, 494, 3028
Neilson, H. R., McNeil, J. T., Ignace, R., & Lester, J. B. 2017, ApJ, 845, 65
Pecaut, M. J., & Mamajek, E. E. 2013, ApJS, 208, 9
Petroni, S., Bono, G., Marconi, M., & Stellingwerf, R. F. 2003, ApJ, 599, 522
Rastorguev, A. S., & Dambis, A. K. 2011, AstBu, 66, 47
Rastorguev, A. S., Dambis, A. K., Zabolotskikh, M. V., Berdnikov, L. N., & Gorynya, N. A. 2013, in IAU Symp. 289, Advancing the Physics of Cosmic Distances, ed. R. de Grijs (Cambridge: Cambridge Univ. Press), 195
Rastorguev, A. S., Lazovik, Y. A., Zabolotskikh, M. V., Berdnikov, L. N., & Gorynya, N. A. 2019, arXiv:1911.10413
Riess, A. G., Casertano, S., Yuan, W., et al. 2018, ApJ, 861, 126
Riess, A. G., Casertano, S., Yuan, W., Macri, L. M., & Scolnic, D. 2019, ApJ, 876, 85
Riess, A. G., Macri, L., Casertano, S., et al. 2011, ApJ, 730, 119
Sabbey, C. N., Sasselov, D. D., Fieldus, M. S., et al. 1995, ApJ, 446, 250
Sachkov, M. E., Rastorguev, A. S., Samus', N. N., & Gorynya, N. A. 1998, AstL, 24, 377
Samus', N. N., Kazarovets, E. V., Durlevich, O. V., Kireeva, N. N., & Pastukhova, E. N. 2017, ARep, 61, 80
Sandage, A. 1958, ApJ, 127, 513
Sasselov, D., & Karovska, M. 1994, ApJ, 432, 367
Storm, J., Carney, B. W., Gieren, W. P., et al. 2004, A&A, 415, 531
Storm, J., Gieren, W., Fouqué, P., et al. 2011, A&A, 534, A94
Turner, D. G. 2010, Ap&SS, 326, 219
Turner, D. G. 2016, RMxAA, 52, 223
Turner, D. G., & Burke, J. F. 2002, AJ, 124, 2931
Udalski, A., & Evans, N. R. 1993, AJ, 106, 348
Wesselink, A. J. 1946, BAN, 10, 91
Ziegler, C., Law, N. M., Baranec, C., et al. 2018, AJ, 156, 259